Journal of Crystal Growth 404 (2014) 223–230

Contents lists available at ScienceDirect

Journal of Crystal Growth

journal homepage: www.elsevier.com/locate/jcrysgro

Crystal growth and characterization of the non-centrosymmetric antiferromagnet $Ba_2CuGe_2O_7$

R. Fittipaldi [a,*], L. Rocco [a], M. Ciomaga Hatnean [b], V. Granata [a], M.R. Lees [b], G. Balakrishnan [b], A. Vecchione [a]

[a] CNR-SPIN Salerno and Department of Physics, University of Salerno, Fisciano (Sa) I-84084, Italy
[b] Department of Physics, University of Warwick, Coventry CV4 7AL, United Kingdom

ARTICLE INFO

Article history:
Received 18 April 2014
Received in revised form
3 July 2014
Accepted 10 July 2014
Communicated by Dr. R.S. Feigelson
Available online 19 July 2014

Keywords:
A1. X-ray diffraction
A2. Floating zone technique
B1. Oxides
B2. Magnetic materials

ABSTRACT

It is well known that non-centrosymmetric tetragonal antiferromagnets can host a number of interesting properties, including multiferroicity as well as magnetic skyrmions and $Ba_2CuGe_2O_7$ is one notable example. The study of all these complex phenomena requires the availability of good crystals. We have carried out the single crystal growth of the helimagnet $Ba_2CuGe_2O_7$ by the floating zone technique, using different gas atmospheres and pressures and report the optimal growth conditions allowing the synthesis of large crystals. X-ray Laue back reflection has been used to determine the orientations of the as-grown crystals. The morphology and chemical composition of the crystals have been investigated by scanning electron microscopy (SEM) with wavelength dispersive spectrometry (WDS). By using powder X-ray diffraction and energy dispersive spectroscopy (EDS) maps, the composition of the starting polycrystalline rods was checked. Powder X-ray diffraction has been also used to check the composition of the grown single crystals. Furthermore, the excellent quality of the $Ba_2CuGe_2O_7$ crystals was confirmed by rocking curve measurements, giving a FWHM of $\sim 0.012^{\circ}$. The crystal growth parameters reported in this work allow the synthesis of high quality single crystals suitable for detailed investigations of the complex magnetic phase diagram of this non-centrosymmetric compound.

1. Introduction

In recent years, the understanding of the multiferroic properties, i.e. of the simultaneous presence of two or more coexisting ferroic orders, has been the topic of increasing interest [1,2]. Indeed, the coexistence in multiferroics of spontaneous magnetization M and polarization P that may respond to relatively weak external electric and magnetic fields respectively, implies potential applications in spintronics devices [3–6]. As a matter of fact, the attention to multiferroics has been mainly driven by the large magnetoelectric (ME) coupling shown by some distorted perovskites of transition metal (TM) oxides displaying both ferroelectric and magnetic properties [7–9]. Furthermore, very recently a so-called spin-dependent hybridization mechanism, where spin-orbit coupling (SOC) induces anisotropic charge-transfer effects between the TM cation and the surrounding oxygens, has been devised for this class of oxides, giving rise to local electric dipoles [10–14]. A necessary ingredient for this mechanism to be realized is the local arrangement of the TM cation with respect to the ligand oxygen, which needs to lack inversion symmetry, e.g. for tetrahedral coordination. The materials with the non-centrosymmetric crystal structure $Ba_2TMGe_2O_7$, consisting of Ge_2O_7 dimers linked by TMO_4 tetrahedra, represent an ideal playground where the properties of TM ions with tetrahedral coordination could be explored in detail [11]. Among this class of compounds, the study of the helimagnet $Ba_2CuGe_2O_7$ is of great interest [15]. This interest has received a further boost due to the theoretical prediction that it could host a lattice of magnetic skyrmions [16], i.e. topologically protected particle-like magnetic "bubbles" with a vortex-like spin texture that could be used for data-storage applications. Nevertheless, up to now no detailed study of the magnetic domains and their microscopic relation to the ferroelectric properties has been performed. For the above reasons, we have attempted to grow large and pure single crystals of $Ba_2CuGe_2O_7$ which can be used to determine its magnetic domain structure.

In this study, we demonstrate the successful growth of high quality $Ba_2CuGe_2O_7$ single crystals using the floating zone (FZ) technique, in different gas atmospheres and pressures. The high crystallinity of the as-grown crystals has been confirmed by high resolution X-ray measurements.

* Corresponding author. Tel.: +39 8996 9147.
E-mail address: fittipaldi@sa.infn.it (R. Fittipaldi).

http://dx.doi.org/10.1016/j.jcrysgro.2014.07.022
0022-0248/

2. Experimental procedures

2.1. Powder synthesis

The starting materials for the preparation of feed and seed rods for growing $Ba_2CuGe_2O_7$ crystals were $BaCO_3$ (Sigma Aldrich 99.999%); CuO (MV Laboratories 99.9999%) and GeO_2 (Alfa Aesar, 99.9999%). The $Ba_2CuGe_2O_7$ polycrystalline rods were prepared by conventional solid state reactions at high temperature. We adopted two different methods, called "A" and "B" in the following, for making single phase polycrystalline rods. In both methods, before the reactions, $BaCO_3$ was pre-annealed at 500 °C for 1 h, and then mixed with the other starting materials, in stoichiometric proportions and heated. In method "A" three thermal treatments at 850 °C for 24 h, 900 °C for 24 h and 950 °C for 15 h with intermediate grindings were performed. After cooling down, the synthesized powder was thoroughly reground and the powder was isostatically pressed for about 10 min in water to a pressure of approximately 50 MPa. The resulting cylindrical rods were sintered in a furnace, in a vertical position, at 980 °C in air for 15 h. In method "B" both the $BaCO_3$, and the GeO_2 were pre-annealed, the latter at 800 °C [17]. The pre-annealing of both $BaCO_3$ and GeO_2 produced dried powders guaranteeing the mixing of the powders in the desired stoichiometry. Moreover, X-ray analysis on GeO_2 powder performed before and after the 800 °C thermal treatment showed a partial transition from α-quartz to the rutile-type structure. It is well known that GeO_2 exhibits several polymorphs [18–21] that mainly differ in their chemical properties, especially solubility and densities. Hence the reaction of GeO_2 in our system, depending on the phase stability and microstructure, is favoured by the thermal treatment. Concerning the method "B", after the pre-annealing, mixtures of starting materials in stoichiometric proportions were heated at 880 °C for 15 h, 950 °C for 20 h and 980 °C for 60 h with intermediate grinding. Finally, the rods were prepared as in the method "A". In both methods, the resulting sintered rods were typically 6–7 mm in diameter and 60–90 mm in length and their densities was determined to be about 85% of the theoretical density of $Ba_2CuGe_2O_7$. Single phase identification was performed by X-ray powder diffraction (XRD).

2.2. Crystal growth

For growing single crystals in this study, we employed the floating zone method using two types of optical image furnaces with elliptical mirrors. One has double-elliptical mirrors (NEC Machinery, model SC1-MDH11020 at CNR-SPIN Salerno) with two 2.0 kW halogen lamps. The other has four elliptical mirrors (Crystal System, model F-ZT-10000-H-IV-VPS at the University of Warwick) with four 500 W halogen lamps. After several attempts of crystal growth, varying the growth conditions, including the speeds of the feed rod and the seed crystal, the counter-rotation speeds and the gas atmosphere, large single crystals with high crystalline quality were obtained. The entire set of growth parameters attempted are summarized in Table 1.

We can see that the rods from method "A" give mixed phase (batches No. 1 and 2) or small crystals (batches No. 3–6) for low growth speed. Improving the quality of the starting polycrystalline rods with method "B", as discussed later, we get bigger and purer crystals (batches No. 8–13). Moreover, from the results summarized in Table 1 we can deduce that the rotation speed, responsible for mixing of material and for the shape of the crystallization front, and the furnace type, strictly related to the temperature distribution within the molten zone [22], greatly influence the size and the colour of the crystals. In fact, comparing the results for batches No. 7 and No. 8 we can see that for the same growth conditions only increasing the rotation speed we change the crystal size. From a comparison of batch No. 8, grown using a two mirror furnace with rotation speeds of 20 rpm, and batch No. 13, grown using a four mirror furnace with a rotation speeds of 30 rpm, we can observe that they show a change in the colour of crystal and this may be related to a combination of two factors: a diverse temperature gradient within the molten zone, related to the different crystal growth furnace used, and to a change of the shape of the crystallization front, due to a change in the rotation speeds. The best results were obtained for a growth rate of 0.5 mm/h, a rotation speed for both rods of 15–30 rpm and an atmosphere of pure O_2 or dried air at a pressure of 5.5 or 3 bar, respectively. It is worth mentioning that the best crystals were obtained starting from feed rods obtained by method "B". This method, as further discussed later in Section 3, assured polycrystalline rods with the right $Ba_2CuGe_2O_7$ phase. This is an important factor in order to achieve a stable liquid zone producing large crystals [22].

2.3. Characterization

The phase composition of the starting polycrystalline rods and of the grown crystals was checked by powder X-ray diffraction using a Bruker D5005 X-ray powder diffractometer employing Cu $K\alpha$ radiation ($\lambda = 1.54$ Å). Rietveld refinement using the FULLPROF code [23] was performed on the θ–2θ scans from 10° to 110° in order to check the phase purity.

Table 1
Summary of crystal quality with varying growth conditions.

Batch No.	Feed rod preparation method	Growth speed (mm/h)	Rotation of feed/seed rods (rpm)	Atmosphere	*P* (bar)	Characteristic of crystal boule
1	**A**	**5**	**40/40**	**Dried Air**	**1**	**Polycrystalline mixed phases**
2	**A**	**5**	**33/33**	**O_2**	**1**	**Polycrystalline mixed phases**
3	**A**	**0.5**	**30/30**	**O_2**	**1**	**Small transparent yellowish crystals**
4	**A**	**1.5**	**10/10**	**Dried Air**	**5.5**	**Small transparent yellowish crystals**
5	**A**	**0.5**	**20/20**	**Dried Air**	**5.5**	**Small transparent yellowish crystals**
6*	**A**	**0.5**	**30/30**	**O_2**	**3**	**Small transparent yellowish crystals**
7	**B**	**0.5**	**10/10**	**O_2**	**3**	**Small dark yellow crystals**
8	**B**	**0.5**	**20/20**	**O_2**	**3**	**Large dark yellow crystals**
9	**B**	**0.5**	**15/15**	**Dried Air**	**5.5**	**Large transparent yellowish crystals**
10	**B**	**0.5**	**25/25**	**Dried Air**	**5.5**	**Large transparent yellowish crystals**
11	**B**	**0.5**	**25/25**	**Dried Air**	**5.5**	**Large transparent yellowish crystals**
12	**B**	**0.5**	**25/25**	**Dried Air**	**5.5**	**Large transparent yellowish crystals**
13*	**B**	**0.5**	**30/30**	**O_2**	**3**	**Large transparent yellowish crystals**

The crystals labelled by the superscript (∗) were grown using a four mirror furnace, while all the other growths were performed employing a two mirror furnace. *P* is total pressure in the quartz tube.

The X-ray Laue back reflection technique was used to orient single crystals specifically for selected experiments. The Laue diffraction experiments were conducted on a high resolution X-ray Laue camera (Photonic-Science). The crystal surface of the oriented samples was inspected by polarized light optical microscopy (PLOM) and by scanning electron microscopy (SEM) (LEO, model EVO 50). The compositional analysis was carried out using wavelength dispersive spectroscopy (WDS). Moreover, the compositional homogeneity of polycrystalline rods synthesized with different methods was checked by acquiring elemental maps with an energy dispersive spectrometer (EDS). The structure and crystalline quality of the crystals were assessed by a high-resolution X-ray diffractometer (Philips, model X' Pert MRD), with a Cu $K\alpha$ source and a four-circle cradle. The magnetization measurements on single crystals, in the temperature range 1.5–300 K, were carried out in a Quantum Design MPMS system in zero field cooled (ZFC) and field cooled (FC) modes in an applied magnetic field of 1000 Oe.

3. Results and discussion

The XRD patterns of both the polycrystalline feed rods and powdered single crystals have been refined with a *P*-4 21*m* space group using the Fullprof Rietveld method [23] and the Inorganic Crystal Structure Database file (ICSD #86844) for the tetragonal $Ba_2CuGe_2O_7$ [24,25]. We first compare the quality of the feed rods obtained by the two different methods "A" and "B" to understand how they influence the crystal growth. Fig. 1 shows the comparison of the XRD results of powders obtained from methods "A" and "B". For the powder from the method "A", the obtained pattern mainly matches with the standard tetragonal $Ba_2CuGe_2O_7$ phase, but some spurious peaks were found (Fig. 1b and c). We tried to extract quantitative results by performing a full profile matching with the FULLPROF code combining the major phase $Ba_2CuGe_2O_7$ with the possible unreacted starting oxides ($BaCO_3$, GeO_2, CuO) or with mixed phases that are likely to be formed during thermal treatments such as $CuGeO_3$, $BaGeO_3$, Ba_2CuO_3, $BaCu_2Ge_2O_7$, $Ba_3Ge_3O_9$ and $BaCuO_2$. Despite many trials we were not able to find a good match with any of these phases because of the very low intensity of the spurious peaks and also because many peaks of the possible secondary phases appear just as a shoulder or overlap with the peaks of the main $Ba_2CuGe_2O_7$ phase.

Nevertheless, from a careful inspection of the spectra we were able to index not only the spurious peaks related to the presence of CuO phase (Fig. 1c) but also some of the peaks not belonging to $Ba_2CuGe_2O_7$ phase as due to the following oxides: $BaCu_2Ge_2O_7$ and $Ba_3Ge_3O_9$ (Fig. 1b). Accordingly, we may conclude that method "A" produces the expected phase $Ba_2CuGe_2O_7$ and a very low amount of $BaCu_2Ge_2O_7$, $Ba_3Ge_3O_9$ and CuO.

For the powder obtained with the method "B", the pattern matches very well with the standard tetragonal $Ba_2CuGe_2O_7$ phase and no undesired peaks were found (Fig. 1d and e). This was further confirmed by the EDS compositional maps. We compared the EDS maps acquired on different pieces of polycrystalline rods obtained via both method "A" and "B". Each sample was mirror polished and, to get a metallic surface, coated with a thin layer ($\sim$20 nm) of silver. In Fig. 2 are shown the elemental maps acquired on a polycrystalline samples obtained via method "A". These show large areas with an homogeneous composition of $Ba_2CuGe_2O_7$ and few small domains rich in copper (Fig. 2, left panel) or with a composition of $BaCu_2Ge_2O_7$ (Fig. 2, right panel), in agreement with the X-ray data. Concerning polycrystalline samples synthesized via method "B" we did not identify any off-stoichiometric domains. A uniform distribution of Ba, Cu, Ge and O atoms in the expected ratio of 2:1:2:7 was observed (Fig. 3).

Of the two different powders obtained, the powder from method "B" therefore appears to be the pure $Ba_2CuGe_2O_7$ phase. This greatly influences the quality of the grown crystal as shown in Table 1. In fact looking at the last column in Table 1 it is evident that the best crystals were achieved starting from feed rods obtained using method "B".

To check the quality of grown crystals, a careful inspection by optical microscopy of all crystal batches listed in Table 1 was performed. We observed that for fast growth speed (batches No. 1 and 2) no single crystals were observable.

The XRD pattern of powdered crystals from batches No. 1 and 2, showed that many diffraction peaks could not be indexed to the $Ba_2CuGe_2O_7$ phase, while some of the peaks were indexed as being related to the presence of Cu_2O phase, which was observable in some areas of the as grown boule as small red patches.

Optical microscopy inspection of crystals batches from No. 3 to No. 6 revealed the presence of small transparent yellowish crystals surrounded by a darker outer layer. From these batches we were able to isolate rectangular shaped transparent yellowish crystals about 4 mm in length and 2×1 mm^2 in cross section. XRD experiments performed on crushed crystals from the growths with the dark layer showed diffraction peaks matching with the $Ba_2CuGe_2O_7$ phase, confirming the single phase nature of these batches.

As reported in Table 1, crystals from batches No. 7 and 8 were characterized by a dark yellow coloured boule. The XRD experiments on these crushed crystals showed diffraction peaks matching with the $Ba_2CuGe_2O_7$ phase. For this reason we believe that the dark colour of the boule does not arise due to a 'secondary phase' but may be due to a slight off stoichiometry of oxygen, though this deserves further investigation.

Finally, optical microscopy investigation revealed the presence of large transparent yellowish crystals for batches No. 9 to No. 13. Crystals about 10 to 20 mm long and roughly 5 to 6 mm in diameter were obtained. A photograph of a crystal boule (batch No. 10) of $Ba_2CuGe_2O_7$ is shown in Fig. 4. We did not observe any natural preference for the crystal boule to cleave and crystals specifically orientated by the Laue technique were cut from the crystal boule for selected experiments.

The XRD patterns and Rietveld refinement of crushed transparent yellowish crystals from the batch No. 12 showed diffraction peaks, all of which could be indexed to the $Ba_2CuGe_2O_7$ phase (Fig. 5), which means that transparent yellowish $Ba_2CuGe_2O_7$ crystals are the pure phase. As there are no reported values of the anisotropic thermal displacement parameters available for the $Ba_2CuGe_2O_7$ phase in our refinement we have used those reported for the $Ba_2CoGe_2O_7$ compound [26]. A careful analysis of our Rietveld refinement shows that the mismatch between the calculated and the measured intensities comes mostly from the limit in the definition of the thermal displacement parameters when refining a pattern obtained using an X-ray laboratory diffractometer. A more accurate evaluation of these parameters needs synchrotron or neutron diffraction patterns. Regardless of the issues with fixing the thermal displacement parameters, we believe that the refinement is of good quality and we are able to determine from the fit the lattice parameters and other structural parameters, such as atomic positions and bond lengths. In Table 2 are summarized the refined lattice parameters obtained for the polycrystalline and single crystal samples. The crystallographic data are in agreement with previously reported values [24,25].

The compositional analysis of the crystals by WDS was carried out on various regions of selected crystals from different batches. We systematically measured the crystal batches with the transparent yellowish colour (batch No. 9–13).

The atomic percentage obtained normalizing WDS data to the stoichiometric value of Ba=2 was $Ba_{2.00\pm0.03}Cu_{1.02\pm0.02}Ge_{2.04\pm0.03}O_{7.2\pm0.1}$.

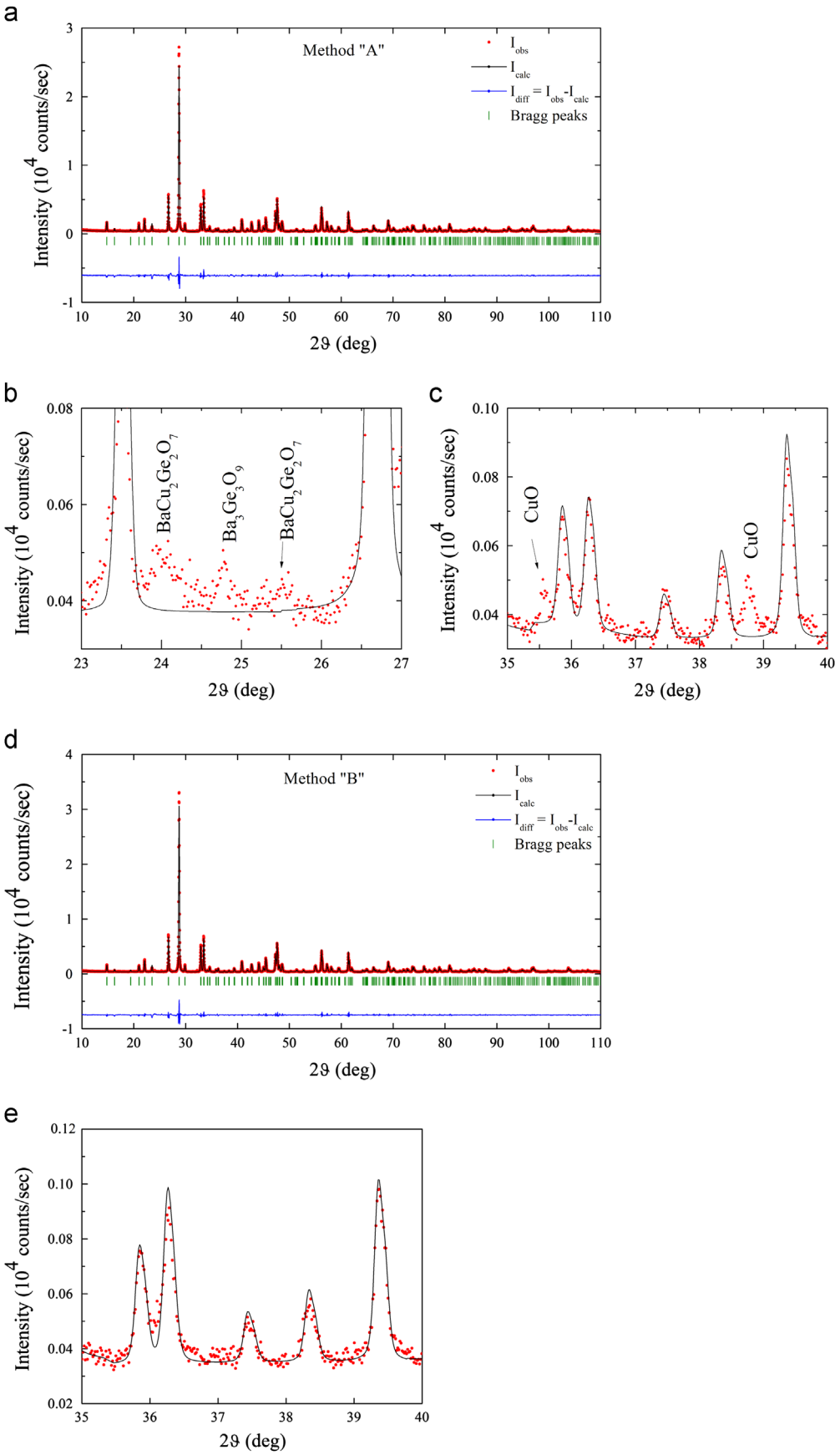

Fig. 1. (a) XRD data refinement of the powder from method "A" and (b) and (c) a zoom of the observed X-ray diffraction patterns along with calculated profiles for $Ba_2CuGe_2O_7$ phase. The spurious peaks have been indexed as being due to mixed oxides formed during thermal treatments; (d) and (e) XRD data refinement of the powder from method "B" and a zoom of the observed diffraction pattern, no spurious peaks from unreacted CuO phase can be seen in this method. In both cases the *P*-4 21*m* space group has been used.

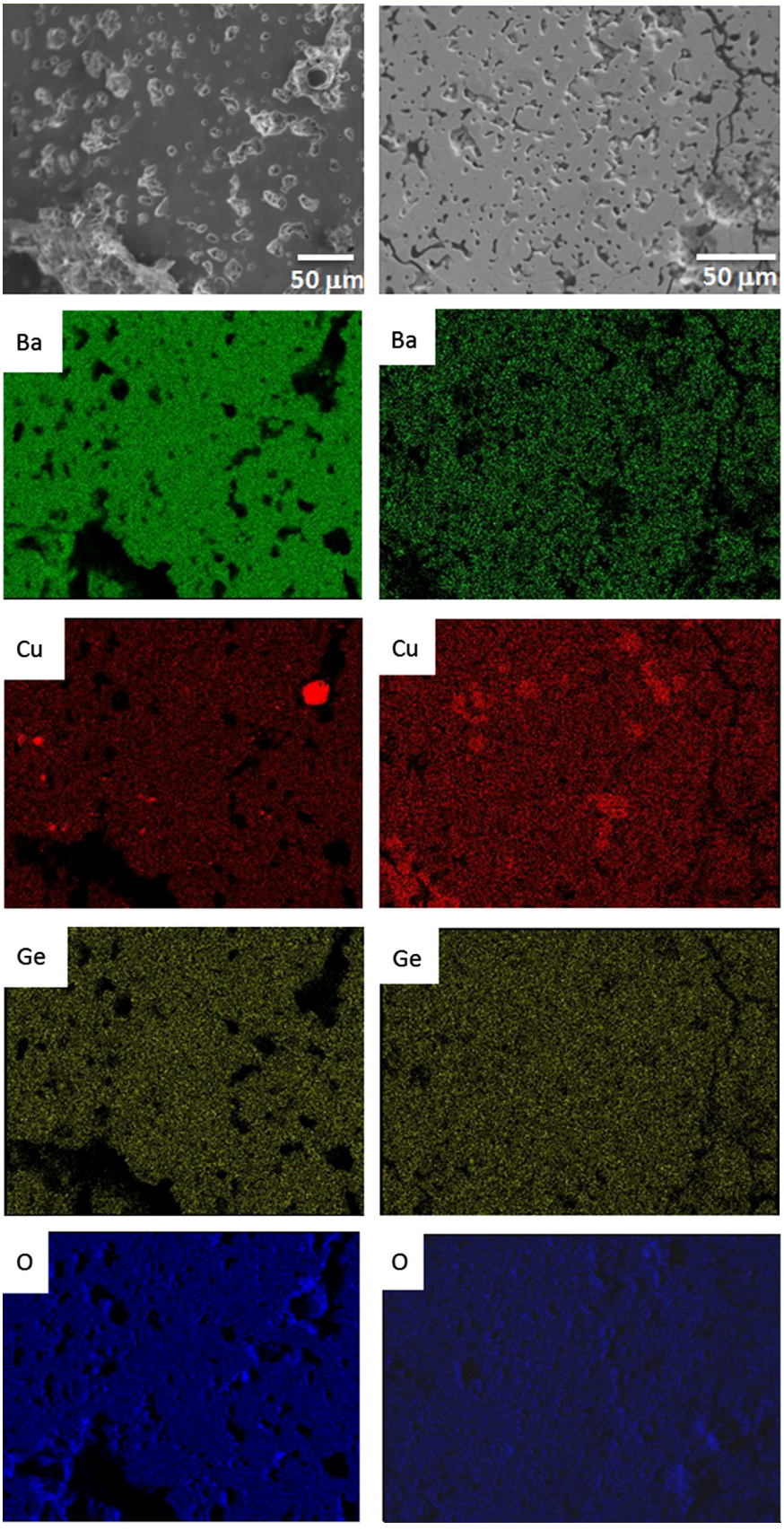

Fig. 2. SEM image and EDS compositional map of $Ba_2CuGe_2O_7$ polycrystalline samples synthesized via method "A". Left panels: small regions with deficiency of Ba and Ge and rich in Cu are visible. Right panels: in the regions rich in Cu a deficiency of Ba is observable, while Ge and O are homogeneous. Quantitative EDS results of these off stoichiometric domains gave the composition of $BaCu_2Ge_2O_7$.

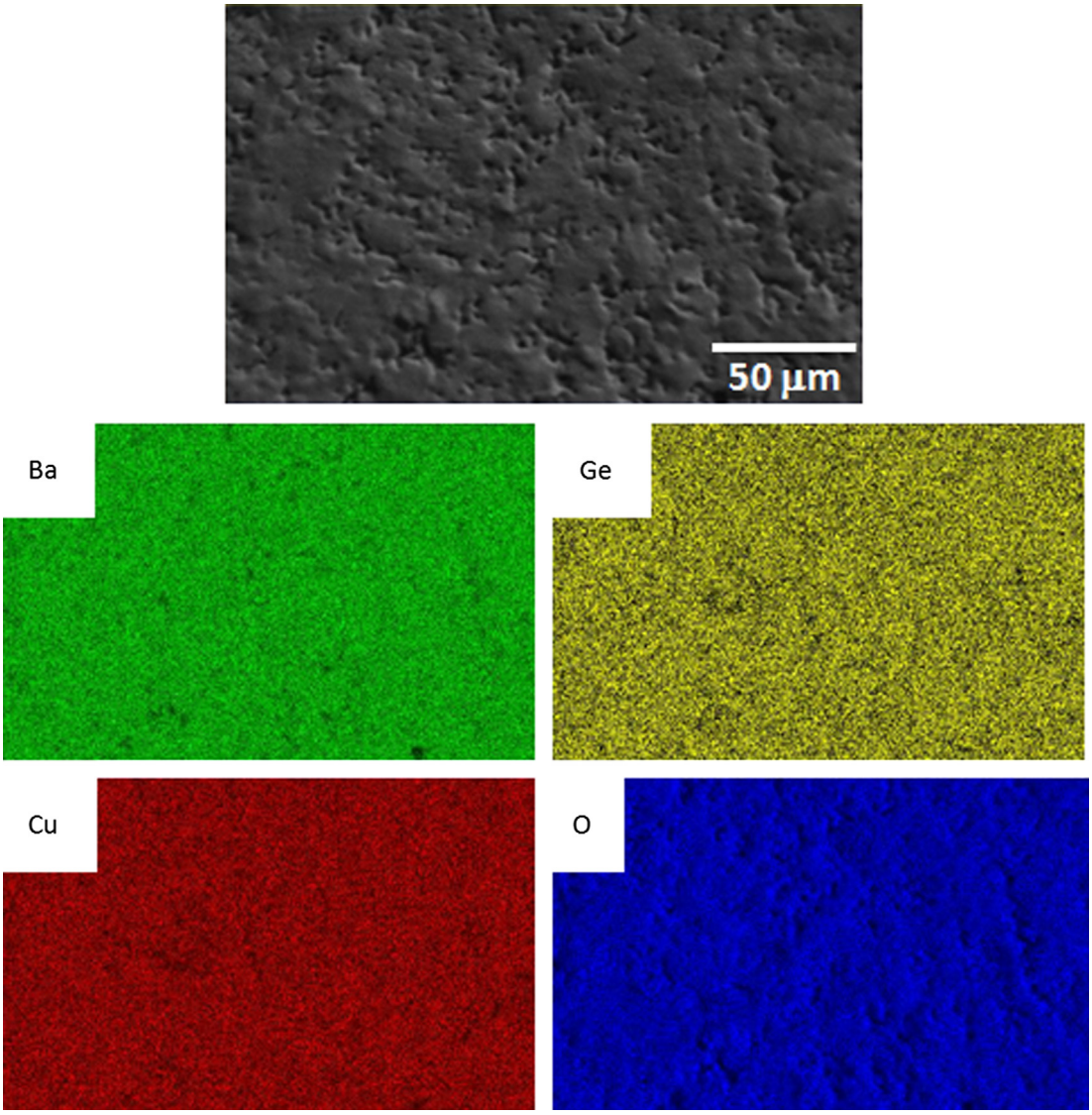

Fig. 3. SEM image and EDS compositional map of a $Ba_2CuGe_2O_7$ polycrystalline sample synthesized via method "B". A uniform distribution of the elements Ba, Cu, Ge and O, corresponding to the expected atomic ratio of 2:1:2:7 has been observed.

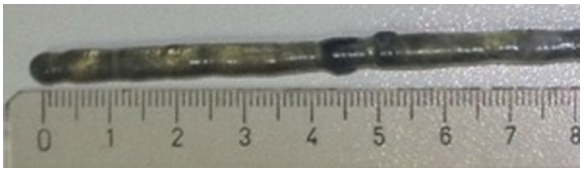

Fig. 4. Photograph of a $Ba_2CuGe_2O_7$ single crystal grown in this work (batch No. 10).

Preliminary WDS analysis on the dark yellow crystals (batches No. 7, 8) revealed an excess of oxygen in these crystals. However, more work is needed to better clarify the exact oxygen stoichiometry of the dark crystals.

Samples of few mm^3 from batches No. 6, 10 and 11 oriented using the X-ray Laue technique, were cut parallel to (0 0 1) or (0 1 0) planes and their surfaces were mirror polished. In Fig. 6 (a) and (b) are shown the Laue photographs of two samples surfaces with (0 0 1) and (0 1 0) planes being orthogonal to the X-ray beam, respectively.

The excellent quality and perfect orientation of the crystals were further confirmed by high resolution X-ray diffraction measurements. In Fig. 7 is shown the rocking curve of the (0 0 2) reflection proving the high crystallinity of the grown $Ba_2CuGe_2O_7$ crystals. After careful mechanical polishing, the same crystals oriented by Laue technique, were also inspected by electron back scattered diffraction technique.

This measurement allowed us to ascertain the absence of any misorientation on a microscopic scale supporting our findings from X-ray measurements.

Finally, magnetization measurements carried out from room temperature down to 1.5 K on single crystals (batch No. 6) in zero field cooled and field cooled conditions, in a magnetic field of 0.1 T are shown in Fig. 8.

These show paramagnetic behaviour of $Ba_2CuGe_2O_7$ samples at room temperature, as reported in literature [27]. Moreover, two separate features are visible in the inset of Fig. 8: a broad peak below $T=10$ K, centred at $T\sim8.5$ K, and a cusp like minimum at $T_N\sim3.3$ K. The broad peak is related to short range antiferromagnetic 2D correlations in the basal (a,b) plane [27], while the increase in the magnetization at low temperature is due to the

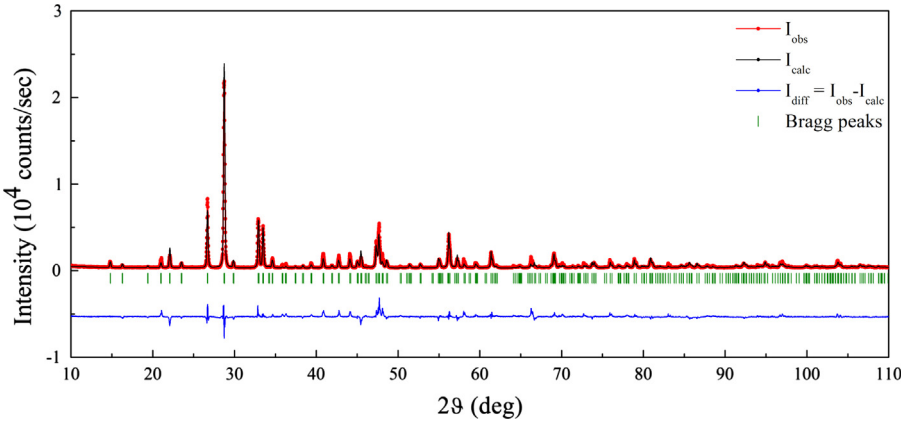

Fig. 5. XRD data refinement of the powder from crushed transparent yellowish crystals (batch No. 12), the *P*-4 21 *m* space group has been used.

Table 2
XRD refinement data of $Ba_2CuGe_2O_7$ samples.

Sample	$a=b$ (Å)	c (Å)	*GOF*	R_p	R_{wp}
Method A	8.45930(5)	5.43940(4)	2.24	6.92	9.40
Method B	8.46023(5)	5.43962(4)	2.10	6.14	8.32
Powdered crystal (batch No. 12)	8.46013(11)	5.44003(7)	3.67	10.9	15.1

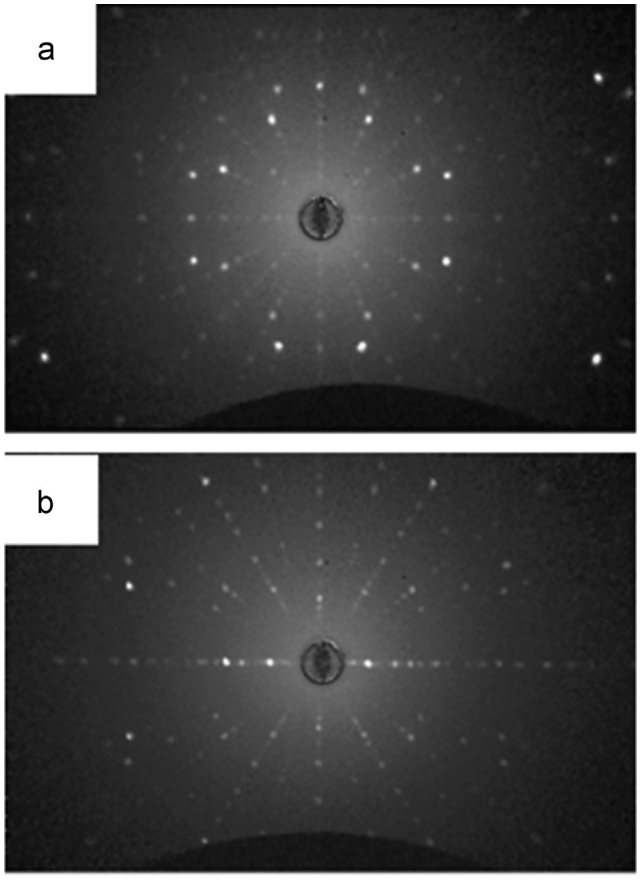

Fig. 6. X-ray Laue patterns of $Ba_2CuGe_2O_7$ crystals oriented with the (a) [0 0 1] (batch No. 10) and (b) [0 1 0] (batch No. 11) direction orthogonal to the exposed surface.

long-range helimagnetic ordering occurring at $T_N=3.3$ K [11]. The observed magnetization in our crystal is consistent with the phase diagram of $Ba_2CuGe_2O_7$ outlined recently by neutron diffraction

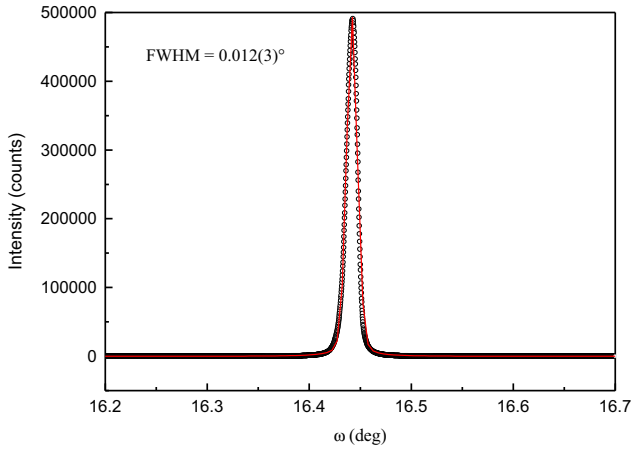

Fig. 7. Rocking curve of the (0 0 2) reflection acquired on a $Ba_2CuGe_2O_7$ single crystal (batch No. 10) The line is a fit with a pseudo-Voigt curve.

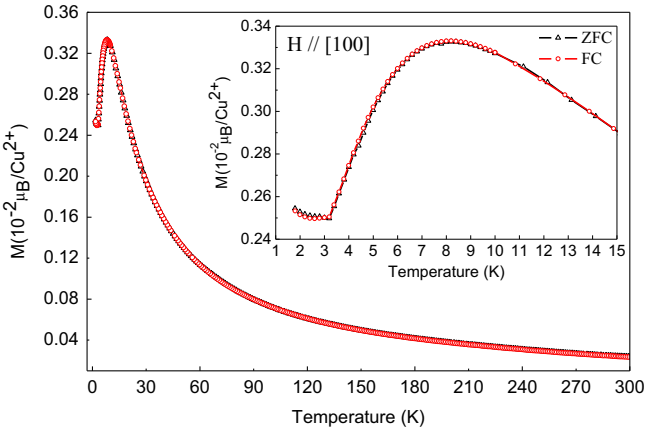

Fig. 8. Magnetization versus temperature of $Ba_2CuGe_2O_7$ single crystal (batch No. 6) for a field $H=0.1$ T applied parallel to the [1 0 0] axis. Inset: enlargement of low temperature magnetic behaviour.

study [28,29] and combined magnetization and polarization measurements [11]. It is worth mentioning that the same magnetic behaviour was observed for the dark yellow crystals (batches No. 7 and 8). We observe the same magnetic behaviour in the transparent crystals obtained from batches No. 9 to 13 and the dark yellow crystals obtained from batches No. 7 and 8, confirming that the different colour of the crystals does not affect their magnetic behaviour. Further studies are needed to clarify the origin of the different colours of the as-grown crystals, which we believe is probably due to some subtle variations in the oxygen stoichiometry.

4. Conclusions

$Ba_2CuGe_2O_7$ single crystals have been successfully grown by the floating zone technique using both two and four mirror optical floating-zone furnaces. The synthesis procedure of the polycrystalline rods was found to be a critical factor for the crystal growth. Two different routes for preparing starting polycrystalline rods, called method "A" and "B", have been compared and the latter method has been shown to produce purer single phase polycrystalline rods crucial for the growth of high quality single crystals. Various crystal growth conditions have been attempted and the optimum conditions to produce the best crystals that emerge from our study are the use of a pure single phase $Ba_2CuGe_2O_7$ starting rod (method "B") and a growth rate of 0.5 mm/h, in air or in a pure oxygen atmosphere at a pressure of 5.5 or 3 bars, respectively. The as grown boules are roughly 8–10 cm in length and 6 mm in diameter from which centimetre size crystals can be selected for experiments. The excellent crystallinity of the crystals obtained is confirmed by the FWHM value of X-ray rocking curve of 0.012°. $Ba_2CuGe_2O_7$ shows a complex magneto-electric behaviour and additionally hosts a number of interesting properties, as well as magnetic skyrmions. Synthesis of large single crystals allows us to investigate the fundamental physics of this material in order to identify the mechanisms responsible for its peculiar multiferroic properties.

Acknowledgements

The authors acknowledge useful discussions with E. Pomjakushina, K. Conder (PSI), O. Petrenko (Warwick), C. Mazzoli (Milan), S. Picozzi, P. Barone and A. Ubaldini (CNR-SPIN). The research leading to these results has received funding from the European Union Seventh Framework Programme (FP7/2007-2013) under grant agreement N. 264098—MAMA.

Work at the University of Warwick was supported by EPSRC, UK (EP/I007210/1) and by the University of Warwick, through a RDF. Some of the equipment used in this research at Warwick was obtained through the Science City Advanced Materials Project, Creating and Characterizing Next Generation Advanced Materials Project, with support from Advantage West Midlands (AWM) and was partially funded by the European Regional Development Fund (ERDF).

References

[1] N.A. Spaldin, M. Fiebig, Science 309 (2005) 391–392.
[2] S.W. Cheong, M. Mostovoy, Nat. Mater. 6 (2007) 13–20.
[3] J.F. Scott, Nat. Mater. 6 (2007) 256–257.
[4] J. Ma, J. Hu, Z. Li, C.W. Nan, Adv. Mater. 23 (2011) 1062–1087.
[5] D. Pantel, S. Goetze, D. Hesse, M. Alexe, Nat. Mater. 11 (2012) 289–293.
[6] J. Allibe, S. Fusil, K. Bouzehouane, C. Daumont, D. Sando, E. Jacquet, C. Deranlot, M. Bibes, A. Barthélémy, Nano Lett. 12 (2012) 1141-1145.
[7] T. Kimura, T. Goto, H. Shintani, K. Ishizaka, T. Arima, Y. Tokura, Nature 426 (2003) 55–58.
[8] N. Hur, S. Park, P.A. Sharma, J.S. Ahn, S. Guha, S-W. Cheong, Nature 429 (2004) 392–395.
[9] M. Gajek, M. Bibes, S. Fusil, K. Bouzehouane, J. Fontcuberta, A. Barthélémy, A. Fert, Nat. Mater. 6, 296-302 (2007).
[10] J.T. Zhang, X.M. Lu, J. Zhou, H. Sun, F.Z. Huang, J.S. Zhu, Phys. Rev. B: Condens. Matter 87 (2013) 075127-1–075127-6.
[11] H. Murakawa, Y. Onose, S. Miyahara, N. Furukawa, Y. Tokura, Phys. Rev. B: Condens. Matter 85 (2012) 174106-1–174106-10.
[12] K. Yamauchi, P. Barone, S. Picozzi, Phys. Rev. B: Condens. Matter 84 (2011) 165137-1–165137-6.
[13] C. Jia, S. Onoda, N. Nagaosa, J. Hoon Han, Phys. Rev. B: Condens. Matter 76 (2007) 144424-1–144424-7.
[14] H. Murakawa, Y. Onose, S. Miyahara, N. Furukawa, Y. Tokura, Phys. Rev. Lett. 105 (2010) 137202-1–137202-4.
[15] H. Murakawa, Y. Onose, Y. Tokura, Phys. Rev. Lett 103 (2009) 147201-1–147201-4.
[16] A.N. Bogdanov, U.K. Rößler, M. Wolf, K.-H. Müller, Phys. Rev. B: Condens. Matter 66 (2002) 214410-1–214410-16.
[17] E. Pomjakushina, K. Conder, PSI Switzerland, Private Communications.
[18] J. Haines, O. Cambon, E. Philippot, L. Chapon, S. Hullz, J. Solid State Chem 166 (2002) 434–441.
[19] A.A. Bolzan, C. Fong, B.J. Kennedy, C.J. Howard, Acta Crystallogr., Sect. B: Struct. Sci 53 (1997) 373–380.
[20] V.V. Atuchin, T.A. Gavrilova, S.A. Gromilov, V.G. Kostrovsky, L.D. Pokrovsky, I.B. Troitskaia, R.S. Vemuri, G. Carbajal-Franco, C.V. Ramana, Cryst. Growth Des 9 (4) (2009) 1829–1832.
[21] M. Micoulaut, L. Cormier, G.S. Henderson, J. Phys. Condens. Matter 18 (2006) R753–R784.
[22] G. Dhanaraj, K. Byrappa, V. Prasad and M. Dudley (Eds.), Springer Handbook of Crystal Growth, "Crystal Growth of Oxides by Optical Floating Zone Technique", chap. 12 (2010) 367–391.
[23] ⟨http://www.ill.eu/sites/fullprof⟩.
[24] www.fiz-karlsruhe.de/icsd.html.
[25] M. Tovar, R.E. Dinnebier, W. Eysel, Mater. Sci. Forum 278 (1998) 750–755.
[26] V. Hutanu, A. Sazonov, H. Murakawa, Y. Tokura, B. Náfrádi, D. Chernyshov, Phys. Rev. B: Condens. Matter 84 (2011) (212101-1 212101-1).
[27] A. Zheludev, G. Shirane, Y. Sasago, N. Kiode, K. Uchinokura, Phys. Rev. B: Condens. Matter 54 (1996) 15163–15170.
[28] S. Mühlbauer, S.N. Gvasaliya, E. Pomjakushina, A. Zheludev, Phys. Rev. B: Condens. Matter 84 (2011) 180406-1–180406-4.
[29] S. Mühlbauer, S. Gvasaliya, E. Ressouche, E. Pomjakushina, A. Zheludev, Phys. Rev. B: Condens. Matter 86 (2012) 024417-1–024417-12.